Journal of Theoretical
and Applied Mechanics
Sofia 1996, Year XXVI No 4

MATHEMATICAL MODELLING FOR A JOINT OF IMPLANTED AND HOST BLOOD VESSELS

I. SELEZOV, O. AVRAMENKO, G. FRATAMICO, G. PALLOTTI, P. PETTAZZONI

Introduction

Analysis of the effect of a vessel joint on the heart pulse propagation is of great importance for organ implantation in general and for blood vessel implantation in particular. The evidence of such a phenomenon has been discovered in [1] on the basis of [2, 3, 4]

A sharp concentration of the axial, hoop and shear stresses takes place in a joint and can essentially influence on a compatibility of organs. Especially dangerous situation can be expected in the case of blood vessel junction due to great pulse reiteration, that can be responsible for developing not only incompatibility.

Analysis of the deformed and stressed state of the anastomotic junction using an isotropic elastic material on the basis of the classical theory of small deformations has been performed in [5]. The recent work [6] indicates that the classical theory overestimates the measured radial change near to the anastomotic junction. More sophisticated model non-linear orthotropic shells is proposed in [7]. The author applied the theory of the linear momentum state superimposed on an initial momentumless state for two arterial locations.

In this study a different approach is accepted. The objective of the work is investigation of the deformation and stress concentration near the suture line caused by the propagation of a short pressure impuls with relatively high amplitude. Such impulses can be connected with so-called "pistol shots" as a result of heart valve insufficiency [8].

Our aim is to develop a physical-mathematical model of the above phenomenon and on this basis to perform qualitative analysis to obtain some quantitative estimations. It is assumed that the pulse reaches the joint and from this initial time $t = 0$ propagates to the right (transmitted wave) and to the left (reflected wave). The corresponding initial boundary value problem is formulated at two regions: the left for the donor vessel of uniform thickness, $-\infty < x \leq 0$, and the right for the host

vessel of uniform thickness, $0 \le x < \infty$. The problem is solved from initial time $t = 0$ for the heart pulse input at $x = 0$. After Laplace transform analytical solutions for two above regions are written and substituted to the matching conditions. Further, a numerical Laplace transform inversion allows to obtain the solutions and provide the qualitative and quantitative analysis.

Statement of the problem

The problem of pulse propagation in an elastic piece-wise vessel consisting of the two perfectly jointed vessels of different thickness is considered (Fig. 1, 2).

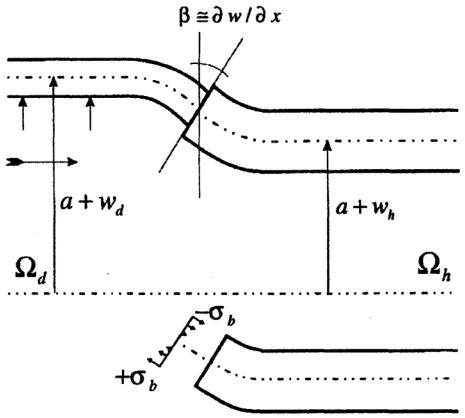


Fig. 1. Bending deformed state of a vessel due to heart pulse propagation. The corresponding moment

$$M \cong \int_{a+w_h}^{a+w_h+h/2} \sigma_b r dr$$

is proportional to h^3.

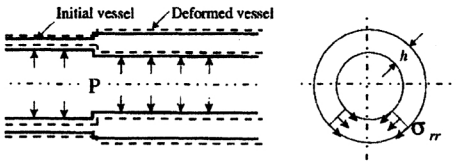


Fig. 2. Traditional model taking into account only the circumferential (chain) stresses σ_{rr} uniformly distributed over the thickness h. The corresponding circumferential force

$$F_\theta^a = \int_{r_i^a}^{r_i^h+h} \sigma_{\theta\theta}^a dr$$

is proportional to h.

The motion of shells is governed by the following differential equations (5)

$$D_d \frac{\partial^4 w_d}{\partial x^4} + \frac{E_d h_d}{a_d^2} w_d + \rho_d h_d \frac{\partial^2 w_d}{\partial t^2} = q_d \quad \text{in } \Omega_d, \tag{1}$$

$$D_h \frac{\partial^4 w_h}{\partial x^4} + \frac{E_h h_h}{a_h^2} w_h + \rho_h h_h \frac{\partial^2 w_h}{\partial t^2} = q_h \quad \text{in } \Omega_h, \tag{2}$$

The fluid motion is governed by the equations [10]

$$\frac{\partial^2 w_d}{\partial t^2} = \frac{r_i^d}{2} \frac{1}{\rho_f} \frac{\partial^2 \hat{p}_d}{\partial x^2}, \tag{3}$$

$$p_i^d = \hat{p}_d - \frac{\left(r_i^d\right)^2}{8} \frac{\partial^2 \hat{p}_d}{\partial x^2}, \quad \text{in } \Omega_d, \tag{4}$$

$$\frac{\partial u_d}{\partial t} = -\frac{1}{\rho_f} \frac{\partial \hat{p}_d}{\partial x}, \tag{5}$$

$$\frac{\partial^2 w_h}{\partial t^2} = \frac{r_i^h}{2} \frac{1}{\rho_f} \frac{\partial^2 \hat{p}_h}{\partial x^2}, \tag{6}$$

$$p_i^h = \hat{p}_h - \frac{\left(r_i^h\right)^2}{8} \frac{\partial^2 \hat{p}_h}{\partial x^2}, \quad \text{in } \Omega_h, \tag{7}$$

$$\frac{\partial u_h}{\partial t} = -\frac{1}{\rho_f} \frac{\partial \hat{p}_h}{\partial x}. \tag{8}$$

The first term in (1) is responsible for the bending deformation (rotation vessel wall) leading to the bending stresses which usually are presented by their integral value such as the bending moment M (Fig. 1). Bending deformation is due to nonuniform distribution of the pulse pressure along the vessel. The second term in (1) is responsible for circumferential (chain) stresses due to internal pressure leading to uniform radial extension (compression) of the vessel (Fig. 2). The third term in (1) takes into account the radial inertia of the vessel wall. It should be noted that in the case of the uniform vessel the most important is only the second term giving dominate contribution. The matching conditions at the interface $x = 0$ are of the form

$$\hat{p}_d = f(t) = \hat{p}_h, \tag{9}$$

$$u_d = u_h, \tag{10}$$

$$w_d = w_h, \tag{11}$$

$$\frac{\partial w_d}{\partial x} = \frac{\partial w_h}{\partial x}, \tag{12}$$

$$D_d \frac{\partial^2 w_d}{\partial x^2} = D_h \frac{\partial^2 w_h}{\partial x^2}, \tag{13}$$

$$D_d \frac{\partial^3 w_d}{\partial x^3} = D_h \frac{\partial^3 w_h}{\partial x^3}, \tag{14}$$

and each searching function $s(x,t)$ should satisfy the following condition

$$|s(x,t)| \to 0, \quad \text{when } |x| \to \infty. \tag{15}$$

The initial conditions are of the form

$$s(x,t)|_{t=0} = 0, \quad \partial s(x,t)/\partial t|_{t=0} = 0. \tag{16}$$

The matching conditions (9-14) express the step of pressures (9), and continuity of fluid velocities (10), shell displacements (11) and their derivatives (12), bending moments (13) and shear forces (14).

Values of the left region d and the right region h (Fig. 1) are labelled with indices d and h, respectively.

The notations of the values in (1-16) are (indices d and h are suppressed)

x — axial coordinate
r — radial coordinate
t — time
w — radial displacement of shell
$\hat{p}$ — mean pressure averaged over the cross-section
$p_i = q$ — radial stress (pressure) on the wall
u — mean velocity
a — radius of the middle surface of shell
h — thickness of shell
E — Young modulus
v — Poisson's ratio
ρ_f — fluid density
ρ — density of vessel material
$D = Eh^3/[12(1-v)]$ — flexured rigidity
$M = D\partial^2 w/\partial x^2$ — bending moment
$Q = D\partial^3 w/\partial x^3$ — shear force
$f(t)$ — pressure pulse.

Equations (1-16) are written in nondimensional form according to the formulas (asterisks are suppressed throughout in the paper)

$$\left(x^*, w_d^*, w_h^*, r_i^{d*}, r_i^{h*}, a, h^*\right) = \left(x, w_d, w_h, r_i^d, r_i^h, a, h\right)/a,$$

$$t^* = \sqrt{E/\rho_f}\,.t/a, \quad \left(u_a^*, u_h^*\right) = \sqrt{\rho_f/E}\,.(u_a, u_h),$$

$$\left(q_d^*, q_h^*, p_d^*, p_h^*, f^*\right) = (q_d, q_h, p_d, p_h, f)/E,$$

$$\left(\rho_d^*, \rho_h^*, \rho_f^*\right) = \left(\rho_d, \rho_h, \rho_f,\right)/\rho_f.$$

It is necessary to note that in all formulas the values $a^* = 1$ and $\rho_f^* = 1$.

Analytical solutions

In the present paper the solutions are obtained by means of the method of Laplace integral transform with further numerical inversion using expansions in sines of even arcs [11].

Laplace transform is determined for any function $s(x, t)$ as

$$S(x,\tau) = \int_0^\infty s(x,t)e^{-\tau t}dt, \tag{17}$$

$$s(x,t) = \int_{-\alpha-i\infty}^{\alpha+i\infty} S(x,\tau)e^{-\tau t}d\tau, \tag{18}$$

and applied to the problems stated above.

In accordance with (17), (18) the equations (1-9) taking into account the initial conditions (16) are reduced to

$$D_d\frac{d^4W_d}{dx^4} + \left(\frac{E_d h_d}{a_d^2} + \rho_d h_d \tau^2\right)W_d = P_i^d, \quad \text{in } \Omega_d \tag{19}$$

$$D_h\frac{d^4W_h}{dx^4} + \left(\frac{E_h h_h}{a_h^2} + \rho_h h_h \tau^2\right)W_h = P_i^h, \quad \text{in } \Omega_h \tag{20}$$

$$\tau^2 W_d = \frac{r_i^d}{2}\frac{1}{\rho_f}\frac{d^2\hat{P}_d}{dx^2}, \tag{21}$$

$$P_i^d = \hat{P}_d - \frac{\left(r_i^d\right)^2}{8}\frac{d^2\hat{P}_d}{dx^2}, \quad \text{in } \Omega_d \tag{22}$$

$$U_d = -\frac{1}{\rho_f}\frac{1}{\tau}\frac{d\hat{P}_d}{dx}, \tag{23}$$

$$\tau^2 W_h = \frac{r_i^h}{2}\frac{1}{\rho_f}\frac{d^2\hat{P}_h}{dx^2}, \tag{24}$$

$$P_i^h = \hat{P}_h - \frac{\left(r_i^h\right)^2}{8}\frac{d^2\hat{P}_h}{dx^2}, \quad \text{in } \Omega_h, \tag{25}$$

$$U_h = -\frac{1}{\rho_f}\frac{1}{\tau}\frac{d\hat{P}_h}{dx}. \tag{26}$$

The matching conditions (9-14) at the interface $x = 0$ are reduced to

$$\begin{aligned} &\hat{P}_d + F(\tau) = \hat{P}_h, && U_d = U_h, \\ &W_d = W_h, && \frac{dW_d}{dx} = \frac{dW_h}{dx}, \\ &D_d \frac{d^2W_d}{dx^2} = D_h \frac{d^2W_h}{dx^2}, && D_d \frac{d^3W_d}{dx^3} = D_h \frac{d^3W_h}{dx^3}. \end{aligned} \tag{27}$$

It follows from (21) and (24) that

$$W_d = \frac{r_i^d}{2\tau^2} \frac{1}{\rho_f} \frac{d^2\hat{P}_d}{dx^2}, \tag{28}$$

$$W_h = \frac{r_i^h}{2\tau^2} \frac{1}{\rho_f} \frac{d^2\hat{P}_h}{dx^2}. \tag{29}$$

Substituting (22), (28) into (19) and (25), (29) into (20) and making some transformations yield the ordinary differential equations of the sixth order for $\hat{P}_d$ and $\hat{P}_h$

$$\frac{d^6\hat{P}_d}{dx^6} + a_1 \frac{d^2\hat{P}_d}{dx^2} + a_2 \hat{P}_d = 0, \tag{30}$$

$$\frac{d^6\hat{P}_h}{dx^6} + b_1 \frac{d^2\hat{P}_h}{dx^2} + b_2 \hat{P}_h = 0, \tag{31}$$

where

$$\begin{aligned} a_1 &= \left(\frac{E_d h_d}{a_d^2} + \rho_d h_d \tau^2 + \frac{r_i^a \tau^2}{4} \right) / D_d, \\ a_2 &= -2\tau^2 / \left(r_i^d D_d \right), \\ b_1 &= \left(\frac{E_h h_h}{a_h^2} + \rho_h h_h \tau^2 + \frac{r_i^h \tau^2}{4} \right) / D_h, \\ b_2 &= -2\tau^2 / \left(r_i^h D_h \right). \end{aligned}$$

Corresponding characteristic equations are bicubic and their roots can be found using the Cardano's formulas. There is a couple of real roots of different signs and two couples of complex-conjugated roots. Let us denote these roots by $\pm l_1$, $\pm l_2$, $\pm l_3$ for (30) and $\pm g_1$, $\pm g_2$, $\pm g_3$ for (31), where $l_1, g_1 > 0$ and l_i and g_i (2, 3) have the positive real parts.

According to this analysis and the conditions (5) the solutions of the equations (30) and (31) can be presented as follows

(32) $$\hat{P}_d = C_1(\tau)e^{l_1 x} + C_2(\tau)e^{l_2 x} + C_3(\tau)e^{l_3 x},$$

(33) $$\hat{P}_h = B_1(\tau)e^{-g_1 x} + B_2(\tau)e^{-g_2 x} + B_3(\tau)e^{-g_3 x}.$$

From (28), (29), (32), (33) and expressions for M the displacements and bending moments are written in the form

(34) $$W_d = \frac{r_i^d}{2\tau^2}\left(C_1(\tau)l_1^2 e^{l_1 x} + C_2(\tau)l_2^2 e^{l_2 x} + C_3(\tau)l_3^2 e^{l_3 x}\right),$$

(35) $$W_h = \frac{r_i^h}{2\tau^2}\left(B_1(\tau)g_1^2 e^{-g_1 x} + B_2(\tau)g_2^2 e^{-g_2 x} + B_3(\tau)g_3^2 e^{-g_3 x}\right),$$

(36) $$M_d = \frac{D_d r_i^d}{2\tau^2}\left(C_1(\tau)l_1^4 e^{l_1 x} + C_2(\tau)l_2^4 e^{l_2 x} + C_3(\tau)l_3^4 e^{l_3 x}\right),$$

(37) $$M_h = \frac{D_h r_i^h}{2\tau^2}\left(B_1(\tau)g_1^4 e^{-g_1 x} + B_2(\tau)g_2^4 e^{-g_2 x} + B_3(\tau)g_3^4 e^{-g_3 x}\right).$$

Substituting the solutions (32-37) into the matching conditions (27) yields the system of algebraic equations to determine unknown coefficients $C_i(\tau)$, $B_i(\tau)$ ($i=\overline{1,3}$).

(38) $$B_1 + B_2 + B_3 - C_1 - C_2 - C_3 = F(\tau),$$

(39) $$g_1 B_1 + g_2 B_2 + g_3 B_3 + l_1 C_1 + l_2 C_2 + l_3 C_3 = 0,$$

(40) $$r_i^h g_1^2 B_1 + r_i^h g_2^2 B_2 + r_i^h g_3^2 B_3 - r_i^d l_1^2 C_1 - r_i^d l_2^2 C_2 - r_i^d l_3^2 C_3 = 0,$$

(41) $$r_i^h g_1^3 B_1 + r_i^h g_2^3 B_2 + r_i^h g_3^3 B_3 + r_i^d l_1^3 C_1 + r_i^d l_2^3 C_2 + r_i^d l_3^3 C_3 = 0,$$

(42) $$D_h r_i^h g_1^4 B_1 + D_h r_i^h g_2^4 B_2 + D_h r_i^h g_3^4 B_3 - D_d r_i^d l_1^4 C_1 - D_d r_i^d l_2^4 C_2 - D_d r_i^d l_3^4 C_3 = 0$$

(43) $$D_h r_i^h g_1^5 B_1 + D_h r_i^h g_2^5 B_2 + D_h r_i^h g_3^5 B_3 + D_d r_i^d l_1^5 C_1 + D_d r_i^d l_2^5 C_2 + D_d r_i^d l_3^5 C_3 = 0.$$

A computer program has been developed for solving the problem. It includes the determination of coefficients from the system (38-43), their substitution into (32-37) and the algorithm of numerical Laplace transform inversion based on the representation of the solutions by expansions in the orthogonal sine functions [11].

Numerical calculations and analysis of results

Numerical calculations have been carried out for the pressure pulse of the form

(44) $$f(t) = At^2 e^{-\alpha t} \quad \text{when } A = 0.5, \quad \alpha = 1.$$

The following results have been obtained:

(a) the pictures of pulse dispersion in uniform hydroelastic system show:

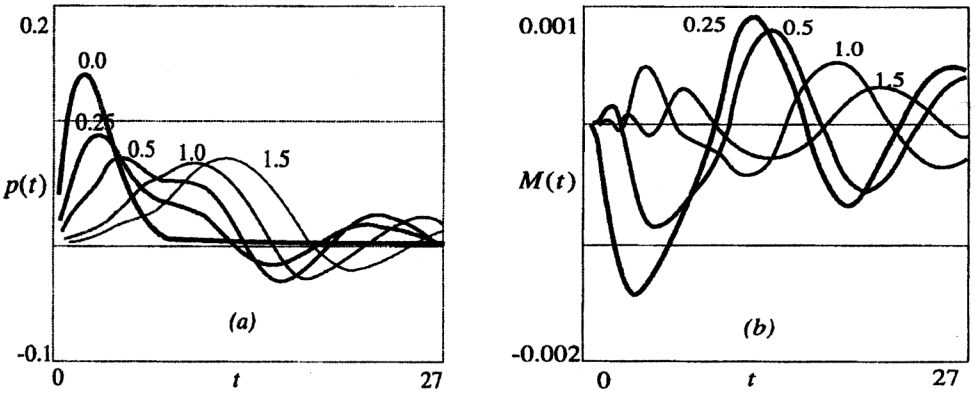


Fig. 3. Pulse evolution in the uniform vessel at the cross-sections:
$x = 0, \pm 0.25, \pm 0.5, \pm 1, \pm 1.5$, when
$h_d = 0.1, E_d = E_h = 1, v_d = v_h = 0.5, \rho_d = \rho_h = 1.1, a = 1$:
(a) the pulse pressure p; (*b*) the bending moment M

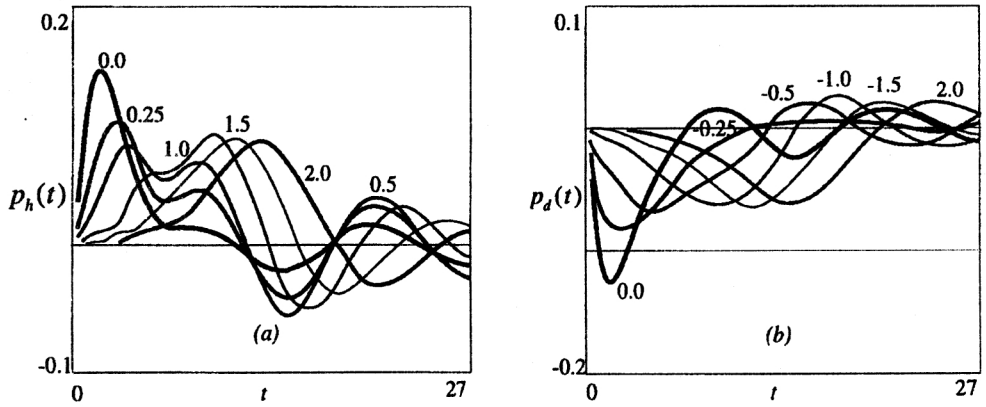


Fig. 4. Evolution of the pulse pressure $p(t)$ for different vessel thicknesses h_d and h_h at the cross-sections:
$x = 0, \pm 0.25, \pm 0.5, \pm 1, \pm 1.5, \pm 2$, when
$h_d = 0.1, h_h = 0.15, E_d = E_h = 1, v_d = v_h = 0.5, \rho_d = \rho_h = 1.1, a_d = a_h = 1$:
(a) the pulse pressure p_h; (*b*)the pulse pressure p_d

— shift the first extremum of $p(t)$ (Fig. 3 a);

— appearance of pressure oscillations in every cross-sections, except $x = 0$;

— oscillations of the bending moment $M(t)$ in cross-sections $x \neq 0$ with the greatest deviations in the cross-section close to $x = 0$ (Fig. 3 b); in the cross-section $x = 0$ the bending moment $M(t) = 0$,

(b) pulse evolution in the jointed vessels (Fig. 4, 5); unlike the uniform system in this case:

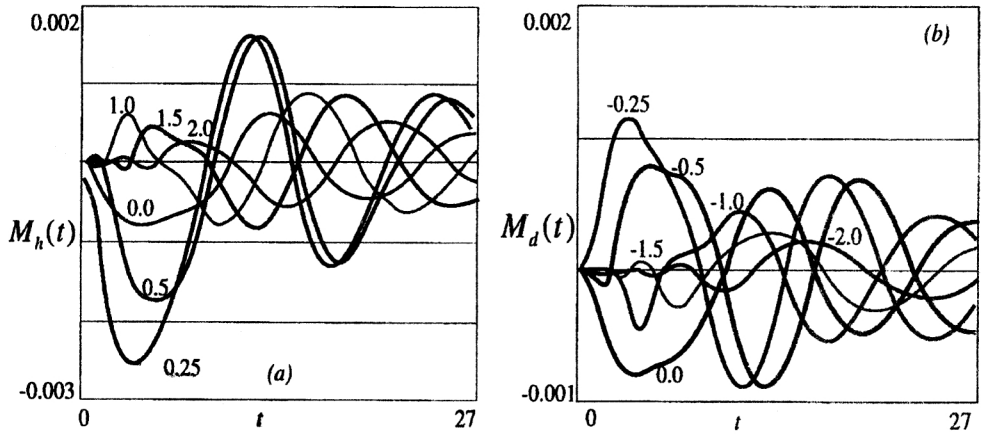


Fig. 5. Evolution of the bending moment $M(t)$ for different vessel thicknesses h_d and h_h at the cross-sections:
$x = 0, \pm 0.25, \pm 0.5, \pm 1, \pm 1.5, \pm 2$, when
$h_d = 0.1, h_h = 0.15, E_d = E_h = 1, \nu_d = \nu_h = 0.5, \rho_d = \rho_h = 1.1, a_d = a_h = 1$:
(a) the bending moment M_h; (*b*) the bending moment M_d

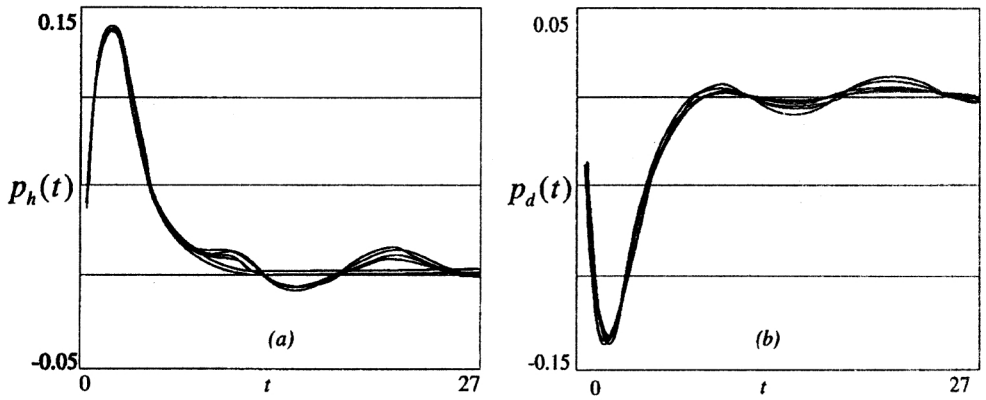


Fig. 6. The influence of the thickness variation on the pulse pressure at the cross-section $x = 0$ when $h_d = 0.1$, $h_h = 0.1025, 0.1050, 0.1075, 0.11, 0.12$,
$E_d = E_h = 1, \nu_d = \nu_h = 0.5, \rho_d = \rho_h = 1.1, a_d = a_h = 1$:
(a) the pulse pressure p_h; (*b*) the pulse pressure p_d

— there are considerable oscillations of both pressure and moment at the cross-section $x = 0$;

— deviations of p_h (Fig. 4a), p_d (Fig. 4b) and M_h (Fig. 5a), M_d (Fig. 5b) are larger in the region Ω_h, where the vessel is thicker,

(c) the dependences of $p(t)$ and $M(t)$ are analysed at $x = 0$ but for different h_h; it is shown that

— initial pulse (approximately finite in time) breaks down into two ones, each of

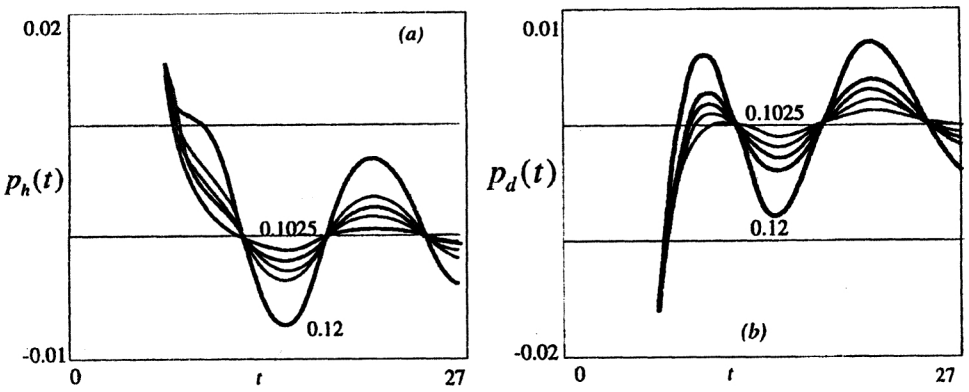


Fig. 7. The dependences $p(t)$ in Fig. 6 in the case of extended vertical scale: (a) the pulse pressure p_h; (*b*) the pulse pressure p_d

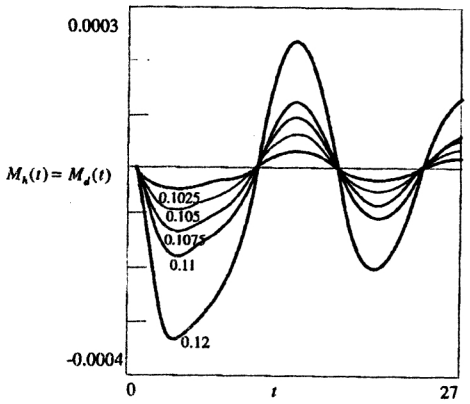


Fig. 8. The influence of the thickness variation on the bending moment at the cross-section $x = 0$ when $h_d = 0.1$, $h_h = 0.1025, 0.1050, 0.1075, 0.11, 0.12$, $E_d = E_h = 1$, $\nu_d = \nu_h = 0.5$, $\rho_d = \rho_h = 1.1$, $a_d = a_h = 1$

them has a great extremum (Fig.6a, Fig.6b) and in further oscillates over a long interval of time (extended pictures Fig.7a, Fig.7b); oscillations increase with increasing h_h (Fig.7a, Fig.7b) and with increasing h_h the moment $M(t)$ in the section $x = 0$ also begins to oscillate, that is not observed in the uniform system when $h_h = h_d$ (Fig.8).

Due to dimensionless parameters introduced the computer program was able to carry out the calculations for the following data: duration of the pulse is about 0.01s (cutting the asymptotic tail with the exactness 10 %); maximum of the given pressure pulse p_{max} = 1.46 kg (force)/cm^2; maximum of the transient pressure in both regions in the case of uniform vessel $p_{max}/2$ = 0.73 kg (force)/cm^2; maximal bending moments for the difference of vessel thicknesses 5 % and 10 % are equal to 0.0004 and 0.0008 kg (force), respectively. Dimension quantities are determined via dimensionless ones as $t = 0.002t^*$s, $p = 5p^*$ kg (force)/cm^2, $M = 5\,M^*$ kg (force).

The values of bending stresses correspond rather the low boundary due to the shortness of pulse considered and the application of the linearized theory valid for

small elastic deformations. Nevertheless, it is interesting to compare the bending stresses predicted by the theory presented here with the circumferential stresses and the stresses of static pre-stressed state.

Here are the formulas used for the calculations of stresses: maximum bending stresses at the outer and inner fibres of vessel wall

$$\sigma_{xx}^{max} = \frac{6}{h^2} M_x^{max}, \tag{45}$$

circumferential stress

$$\sigma_{\theta\theta}^{max} = p_{syst}^{max} \frac{a}{h}, \tag{46}$$

stress of the pre-stressed state

$$\sigma_{\theta\theta}^{max} = p_{tm} \frac{a}{h}. \tag{47}$$

Calculations have been carried out for the following parameters: the wall thickness h =0.001m, radius of the middle surface a = 0.01m, maximum systolic pressure p_{syst}^{max} =20000 n/m^2, pressure of the pre-stressed state p_{tm} = 4000 n/m^2 [12], M_x^{max}= 8000 n (for the thickness difference 10 %).

From the formulas (45-47) for numerical values given above the following results are obtained: σ_{xx}^{max} = 48000n/m^2, $\sigma_{\theta\theta}^{max}$ =200000n/m^2, σ_{xx} = 40000n/m^2.

These results show that the bending deformations near the vessel joint need to be taken in consideration and it is necessary to conduct experimental investigations in the future.

Conclusions

1. Difference of the wall thicknesses of jointed vessels leads to appearance of the bending moment in a joint unlike the case of uniform vessel (Fig. 8);
2. Variation of the wall thickness at 2.5 % can increase the bending moment two time in the location of a joint (Fig. 8, curve 0.1025 and curve 0,1050);
3. The greatest extremum of the bending moment takes place close to a joint due to the pressure step applied to the joint location (Fig. 5, curves 0,25);
4. Similarly, in the case of uniform vessel the greatest extremum of the bending moment takes place close to the joint (Fig. 3b, curve 0,25);
5. The bending moment is redistributed so that the greater extremum takes place in the thicker vessel (Fig. 5);
6. The difference of jointed vessel generates considerable oscillations of the pressure and bending moment (Fig. 4, Fig. 5);

7. The bending stresses in a joint can be the order not less than one for the pre-stressed state due to the background pressure in vessel.

REFERENCES

[1] De Sanctis, L. B., L. Coli, G. Cianciolo et al. A Mathematical Hypothesis for Renal Arterial Stenosis in Renal Transplantation, Biofluid Mechanics, 1994, 421-7.

[2] Corsini, F., G. Pallotti, T. Posteli. Mechanical Biocompatibility in Transplantation. *International Journal of Artificial Organs*, (1984), No 7, 167-71.

[3] Pallotti, G., L. Coli, P. Pettazzoni et al. Renal Arterial Stenosis in Renal Transplantations: A Mathematical Pathogenetic Hypothesis and Its Possible Implications, In: Biofluid Mechanics: Blood Flow in Large Vessels (Ed. D. Liepsh), München, Springer-Verlag, 1994.

[4] Selezov, I. T., G. Pallotti, O. V. Avramenko. Predominant Danger of Bending Stresses in a Joint of an Artificial and Host Blood Vessels. *International Journal of Artificial Organs*, (1995), No **8**, 439.

[5] Paasche, P. E. et al. Consideration of Suture Line Stresses in the Selection of Synthetic Grafts for Implantation. *J. Biomechanics*, **6** (1973), 253-259.

[6] Rodgers, V. G. et al. Experimental Determination of Mechanical Shear Stress About an Anastomotic Junction. *J. Biomechanics*, **20** (1987), 795-803.

[7] Rachev, A. Analysis of the Deformed and Stressed State of the Arterial Vessels, Connected to Synthetic Prostheses. *Biomechanics*, Vol. **21** (1988), 35-48 (in Bulgarian).

[8] Anliker, M., R. Rockwell, E. Ogden. Nonlinear Analysis of Flow Pulses and Shock Waves in Arteries. **I** and **II**, *ZAMP*, 1971, 217-246, 563-581.

[9] Selezov, I. T. Modelling of Wave and Diffraction Processes in Continuous Media, Kiev, Naukova Dumka, 1989 (in Russian).

[10] Moodie, E. B., D. W. Barday, R. T. Tait. A Boundary Value Problem for Fluid-filled Viscoelastic Tubes. *Mathematical Models*, (1983), **4**, 195-207.

[11]Selezov, I. T. Numerical Laplace Transform Inversion for Solving Initial Boundary Value Problems of Mechanics, The 3rd Int. Congress on Industrial and Apl. Math., Hamburg, Germany, 3-7 July 1995, 435.

[12] Pedley, T. J. The Fluid Mechanics of Large Blood Vessels, Cambridge, Cambridge University Press, 1980.